Holistic Coupled Field and Circuit Simulation

Wim Schoenmaker*
Peter Meuris*
*Magwel NV, Leuven, Belgium
Email: {wim.schoenmaker, peter.meuris}@magwel.com

Christian Strohm†
Caren Tischendorf†
†Humboldt Universität zu Berlin, Dept. of Math., Germany
Email: {strohmch, tischendorf}@math.hu-berlin.de

***Abstract*—Circuit simulators used in semiconductor industry are based on lumped element models described in form of net lists. In order to be able to incorporate the mutual electromagnetic influence of neighboring elements (e.g. cross talking), one needs refined models based on a sufficiently exact discretization of the full Maxwell equations. Here, we present a holistic simulation approach for lumped circuit models including 3D electromagnetic field models for specific devices.**

I. Modeling

A. Electromagnetic Field Modeling

The electromagnetic fields can be described by the full-wave Maxwell's equations in potential formulation, see e.g. [1]

$$\nabla \cdot (\varepsilon \nabla \varphi + \varepsilon \vec{\Pi}) = -\varrho \tag{1}$$

$$\nabla \times (\nu \nabla \times \vec{A}) + \partial_t (\varepsilon \nabla \varphi + \varepsilon \vec{\Pi}) = \vec{J} \tag{2}$$

with the scalar potential φ and the vector potential $\vec{A}$ as well as the pseudo-canonical momentum $\vec{\Pi} = \partial_t \vec{A}$ to avoid the second-order time derivative. The material dependent parameters ε and $\mu = \nu^{-1}$ are the permittivity and the magnetic permeability. The charge ϱ and the current density $\vec{J}$ are given by the following model equations:

$$\varrho = \begin{cases} 0 & \text{for metal and isolator} \\ q(n - p - N_D) & \text{for semiconductor} \end{cases} \tag{3}$$

and

$$\vec{J} = \begin{cases} -\sigma \left(\nabla \varphi + \vec{\Pi} \right) & \text{for metal} \\ \vec{J_n} + \vec{J_p} & \text{for semiconductor} \\ 0 & \text{for isolator} \end{cases} \tag{4}$$

with the electron and hole current densities $\vec{J_n}$ and $\vec{J_p}$ as well as the electron and hole concentrations n and p satisfying

$$q_e \partial_t n - \nabla \cdot \vec{J_n} + q_e R(n,p) = 0 \tag{5}$$

$$q_e \partial_t p + \nabla \cdot \vec{J_p} + q_e R(n,p) = 0 \tag{6}$$

with

$$\vec{J_n} = q_e D_n \nabla n - q_e \mu_n n \nabla \varphi, \;\; \vec{J_p} = -q_e D_p \nabla p - q_e \mu_p p \nabla \varphi.$$

The material depending parameters N_D, σ, μ_n and μ_p describe the doping concentration, the conductivity, the mobility of electrons and the mobility of holes. The function R gives the recombination rate for electrons and holes. Finally, q_e is the elementary charge and D_n, D_p are the diffusion coefficients.

Note that the semiconductor current density model reflects the drift-diffusion model [2] and may be extended by an additional current density part caused by the self-induced Lorentz force in case of circuits with ultra-fast transient signals, see [3].

B. Lumped Circuit Modeling

The common approach for simulating circuits is the modified nodal analysis. It bases on the Kirchhoff's laws described by

$$A\vec{i} = 0, \qquad \vec{v} = A^\top \vec{e} \tag{7}$$

with the incidence matrix A mapping branches to nodes of the circuit. The circuit variables are the vector $\vec{i}$ of all branch currents, the vector $\vec{v}$ of all branch voltages and the vector $\vec{e}$ of all nodal potentials. They are completed by the constitutive element equations

$$\vec{i}_1 = \tfrac{\mathrm{d}}{\mathrm{d}t} q(\vec{v}_1, t) + g(\vec{v}_1, t), \quad \vec{v}_2 = \tfrac{\mathrm{d}}{\mathrm{d}t} \phi(\vec{i}_2, t) + r(\vec{i}_2, t) \tag{8}$$

for lumped current and voltage controlling elements, respectively. Notice, all basic types as capacitances, inductances, resistances and sources are covered by a suitable choice of the functions q, g, ϕ and r. Performing the modified nodal analysis, we get the following reduced equation system having only the nodal potentials e and the currents i_2 of the voltage controlling elements, see [4]:

$$A_1 \tfrac{\mathrm{d}}{\mathrm{d}t} q(A_1^\top \vec{e}, t) + A_1 g(A_1^\top \vec{e}, t) + A_2 \vec{i}_2 = 0, \tag{9}$$

$$\tfrac{\mathrm{d}}{\mathrm{d}t} \phi(\vec{i}_2, t) + r(\vec{i}_2, t) - A_2^\top \vec{e} = 0, \tag{10}$$

where the incidence matrix $A = (A_1, A_2)$ is split with respect to the current and voltage controlling elements. The equations (9)-(10) are generated automatically from net lists providing the node to branch element relation (for entries of A_1 and A_2) as well as the element related functions q, g, ϕ and r.

C. Coupled Modeling

We assume the interface between the electromagnetic field model and the lumped circuit model to be perfectly electric conducting such that $\vec{B} \cdot n_\perp = 0$ and $\vec{E} \cdot n_\parallel = 0$ with $n_\perp$ and $n_\parallel$ being the outer unit normal vectors transversal and parallel to the contact boundary. This motivates the boundary conditions, cf. [5],

$$(\nabla \times \vec{A}) \cdot n_\perp = 0, \qquad (\vec{\Pi} + \nabla \varphi) \cdot n_\parallel = 0. \tag{11}$$

978-3-9815370-6-2/DATE16/

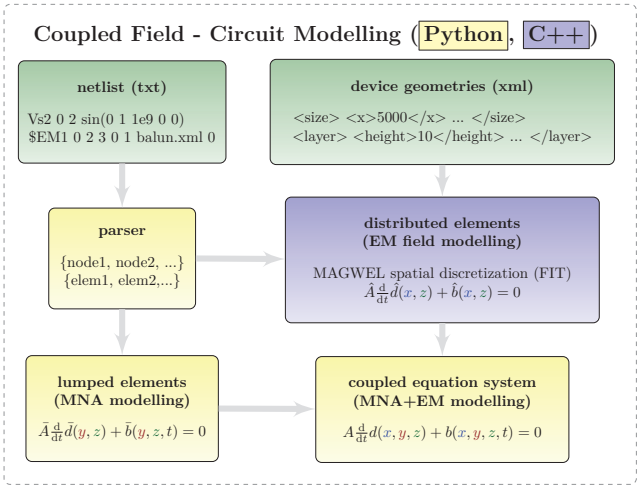

Fig. 1. Holistic modeling of field and lumped elements. The netlist contains all elements. Elements that shall be modeled by EM fields are marked with a $ in the first position. The geometric and material structure is given in the corresponding xml file listed in the same line. The MAGWEL simulator provides the spatially discretized field equations as a DAE system 1. The lumped elements and the connections of all are modeled by MNA resulting in DAE system 2. Finally, the DAE systems are coupled to the holistic field circuit model DAE.

Denoting by Γ_k the k-th contact of the electromagnetic field model element with Γ_0 being the reference contact we get the current through Γ_k as

$$\vec{i}_k = \int_{\Gamma_k} [\vec{J} - \partial_t(\varepsilon(\nabla\varphi + \vec{\Pi}))] \cdot n_\perp \, \mathrm{d}\sigma$$

with $\vec{\Pi} := \partial_t \vec{A}$. Note that equation (4) and the boundary condition (11) guarantee that the sum of all contact currents equals zero, that means

$$\sum_k \vec{i}_k = 0.$$

This model property is necessary for all lumped element descriptions in order to preserve the Kirchhoff's current law. In order to reveal the relation to the voltages $\vec{v}_k$ between the contact Γ_k and the reference contact Γ_0, we express the potential φ as

$$\varphi(x,t) = \varphi_{bi}(x) + \varphi_c(x,t) \tag{12}$$

with the contact potential

$$\varphi_c(x,t) = \begin{cases} \vec{v}_k & \text{if } x \in \Gamma_k \\ 0 & \text{else.} \end{cases}$$

Here, we assumed the reference contact Γ_0 to be the mass node for simplicity. The potential φ_{bi} describes the position dependent built-in potential arising by varying doping concentrations and bonding different materials.

II. Holistic Simulation with Adaptive Time Step Control

In contrast to [6] and [7], where a co-simulation approach is presented, we consider a holistic simulation approach with an adaptive time step control for the whole coupled system.

First, we perform a spatial discretization of the electromagnetic field devices. Afterwards, we apply an adaptive time stepping scheme to the resulting coupled differential-algebraic equation system.

A. Spatial Discretization

The spatial discretization can be seen as a generalized finite-integration technique (FIT). Whereas Gauss' law is at the core of the finite-volume method and the regular finite-integration technique, we note that Gauss' law is a specific case of Stokes' law (13)

$$\int_\Omega \mathrm{d}\omega = \oint_{\partial\Omega} \omega \qquad \text{generalized Stokes} \tag{13}$$

applied to three-dimensional volume elements bounded by two-dimensional closed surfaces :

$$\int_V \nabla \cdot \vec{X} \, \mathrm{d}^3 v = \oint_{\partial V} \vec{X} \cdot \mathrm{d}\vec{S} \quad \text{Gauss}'\text{law} \tag{14}$$

Stokes' theorem is best known as used for two-dimensional surface elements bounded by closed lines :

$$\int_S \nabla \times \vec{X} \cdot \mathrm{d}\vec{S} = \oint_{\partial S} \vec{X} \cdot \mathrm{d}\vec{l} \quad \text{Stokes}'\text{law} \tag{15}$$

We may now apply equations (14) and (15) to the volume cells and surface elements of any unstructured grid in three dimensions. For example the electrostatic Gauss' law $\nabla \cdot \vec{D} = \rho$ with $\vec{D} = \epsilon\vec{E}$ will result into

$$-\int_{\partial\Delta V_i} \epsilon \left(\nabla\varphi + \vec{\Pi}\right) \cdot \mathrm{d}^2\vec{S} = \int_{\Delta V_i} \varrho \, \mathrm{d}^3 v = Q_i \tag{16}$$

The integration over the closed surface is fragmented into summing the contribution of the surface elements (dual areas) where it is assumed that for each fragment the integrand is constant. It should be noted that obtuse elements are possible but their presence may jeopardize the solving procedure because they will push away the linear systems away from diagonal dominance. The next step is to assign unique expressions to $\nabla\varphi$ and $\vec{\Pi}$. This is done by approximating the first by the voltage difference between the endpoints of the links that pierce the dual surface fragments divided by the link length. The second variable is approximated by the projected of the time derivative of the vector potential on the link orientation of the link piercing the dual surface fragment.

$$\nabla\varphi \simeq \frac{\varphi_j - \varphi_i}{h_{ij}} \;, \quad \Pi_{ij} \simeq \vec{\Pi} \cdot \vec{e}_{ij} \tag{17}$$

This brings us to an important aspect of the discretization scheme; the degrees of freedom are: 1) the values of the electrical potential at each grid node 2) the values of the projection of the vector potential on each grid link 3) the first-order time derivatives there off. Furthermore, the values of the

electron and hole Fermi potentials are also stored as degrees of freedom.

Maxwell-Ampere Equation: In order to discretize the Maxwell-Ampere equation, we consider a surface element of the computational grid and consider Stokes' law (15) for this element

$$\int_{\Delta S_i} \nu \nabla \times \vec{B} \cdot \mathrm{d}^2\vec{S} = \int_{\Delta S_i} \left(\vec{J} + \partial_t \vec{D}\right) \cdot \mathrm{d}^2\vec{S} \qquad (18)$$

The left-hand side is rewrittten as :

$$\int_{\Delta S_i} \nu \nabla \times \vec{B} \cdot \mathrm{d}^2\vec{S} = \oint_{\partial \Delta S_i} \nu \vec{B} \cdot \mathrm{d}\vec{l_i} \qquad (19)$$

The line element $\mathrm{d}\vec{l_i}$ is piercing though a primary surface. The right-hand side of (19) is the sum of all line segments that constitute the circumference of ΔS_i. Now $\vec{B}$ is not a degree of freedom. Therefore we apply (15) once more using $\vec{B} = \nabla \times \vec{A}$ for each primary surface :

$$\vec{B} \simeq \frac{1}{\Delta S_i} \oint_{\partial \Delta S_i} \vec{A} \cdot \mathrm{d}\vec{l'} \qquad (20)$$

As a consequence, the left-hand side of (18) is a weighted sum over A_{ij} with the weights determined by the material parameter ν, geometrical factor induced by the grid and by the locality of links being present in nearest-neighboring primary volume elements. The right-hand side of (18) is dealt with in the same as was done for eq. (17). Besides these discretization details a regularization of the gauge conditions is required. Further details can be found in [3].

The resulting system is a DAE system of the form

$$\hat{A}\frac{\mathrm{d}}{\mathrm{d}t}\hat{d}(x,z) + \hat{g}(x,z,t) = 0 \qquad (21)$$

where x contains the potentials φ at the mesh nodes and the vector potentials $\vec{A}$ as well as the pseudo-canonical momenta $\vec{\Pi}$ at the mesh edges. The variable z contains the node potentials and currents at the contacts of the devices.

The MNA equations described in 9-10 do not contain spatial derivatives and can be comprised as a system of the form

$$\bar{A}\frac{\mathrm{d}}{\mathrm{d}t}\bar{d}(y,z) + \bar{g}(y,z,t) = 0. \qquad (22)$$

The vector y contains the nodal potentials and currents (of voltage controling elements) of the lumped circuit. The variable z describes again the node potentials and currents at the contacts of the devices modeled by 3D field equations.

B. Time Discretization

We combine the field DAE system (21) and the circuit DAE system (22) to the system

$$A\frac{\mathrm{d}}{\mathrm{d}t}d(x) + g(x,t) = 0$$

is solved by the BDF methods (cf. [8]), i.e. we solve the nonlinear systems

$$\frac{1}{h_n}\sum_{i=0}^{k} \alpha_{ni} A d(x_{n-i}, t_{n-i}) + g(x_n, t_n) = 0$$

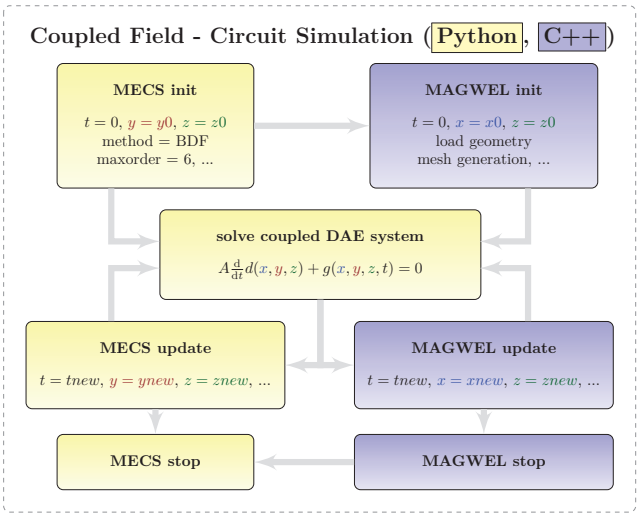

Fig. 2. Flow diagram for the coupled field circuit simulation. It is realized in a Python framework including C++ implementations of the field solver MAGWEL.

at each time point t_n. Here, $h_n := t_n - t_{n-1}$ is the time stepsize,

$$\alpha_{ni} = \frac{t_n - t_{n-1}}{t_n - t_{n-i}} \prod_{j=1, j\neq i}^{k} \frac{t_n - t_{n-j}}{t_{n-i} - t_{n-j}}, \quad i = 1, ..., k,$$

$$\alpha_{n0} = -\sum_{i=1}^{k} \alpha_{ni},$$

are the BDF coefficients and x_{n-i} are the numerical approximations of the exact solution $x(t_{n-i})$ at the time points t_{n-i}. The implemented time integration scheme has the option to switch to a Runge Kutta scheme (Radau IIa), cf. [9], for starting and restarting the integration.

The adaptive time step control estimates the error for the dynamic components $d(x_n, t_n)$. As reported in [10], [11], such a control is more stable and reliable for higher index DAE systems. The error is estimated by the difference of $d(x_n, t_n)$ and $d(x_n^p, t_n)$ with x_n^p being the predictor

$$x_n^p := \sum_{i=1}^{k+1} \gamma_{ni} x_{n-i}$$

and

$$\gamma_{ni} := \prod_{j=1, j\neq i}^{k+1} \frac{t_n - t_{n-j}}{t_{n-i} - t_{n-j}}, \quad i = 1, ..., k+1.$$

III. Implementation Issues

The flow of the coupled simulation is shown in Figure 2. It is realized in a Python framework including C++ implementations of the field solver MAGWEL. First the circuit solver MECS and the field solver MAGWEL are initialized. The MECS init includes information about the initial data, the time interval, the type of DAE solver, the order of the method, the

```
Rs1 0 1 50
Vs2 0 2 sin(0 1 1e9 0 0)
Vs3 0 3 sin(0 1 -1e9 0 0)
$EM1 0 2 3 0 1 structure_balun.xml 0
```

Fig. 3. Net list with a $-line that triggers a field solving approach for a netlist element. The example line is read as follows: There is a net list element with name EM1 whose field solver details can be found in the file structure_balun.xml. The five outer contacts of this element are connected to the nodes 0, 2, 3, 0 and 1. The last number in the line refers to the reference contact (usually the mass node).

initial stepsize and other controlling information for the circuit solver. The MAGWEL init comprises the load of the geometry, the generation of a mesh and further controlling information for the field solver. After the initial phase, the coupled DAE system is formed as described in Figure 1 and solved for one time step. Then, a new stepsize is determined using an error estimator for the time discretization error. Afterwards, the circuit and the field solver are updated with data corresponding to the new time point t_{new} and the recent solution x_{new}, y_{new}, z_{new}. This allows a further time step, i.e. the coupled DAE system is solved again. This loop is continued until the final time point has reached.

Note, from the circuit simulator's perspective a new element is defined that triggers the use of the field solver for the generation of the field equations on a computational grid. The syntax is illustrated in Figure 3 and must be read as follows: There is a net list element with name EM1 whose field solver details can be found in the file structure_balun.xml. The contacts of this element are connected to the nodes 0, 2, 3, 0 and 1. The last number in the line refers to the reference contact (usually the mass node).

IV. Test Benchmark: Simple Circuit with Balun Device

We consider a simple circuit with a balun device given in Figure 4. The RF input signals V_{S2} and V_{S3} are sinusoidal ones operating with 1GHz frequency, see Figure 6. The RF output is given as current through the resistance R_{S1}, see Figure 7.

A detailed view of the balun structure is shown in Figure 5 The top coil is an open circuit and a single GSG port (P1) is attached. The balanced bottom coil (single winded) has a GSGSG 2-port (P2 and P3) connection.

In the following we present our results for the holistic transient simulation of the test circuit, see Figure 4, yielding 133 171 equations for the coupled differential-algebraic system to be solved. Due to the high computational effort (about 30min per time step), we restricted the simulation to a rough tolerance of $1e-2$. The currents at the three ports $P1$, $P2$ and $P3$ can be seen in Figure 7. The output voltage at port P1 is shown in Figure 8. Furthermore, we see in Figure 9 and Figure 10 the vector potentials at the first two edges and their pseudo-canonical momenta. We observe some instability at the time points around $1.7e-10$. So far, we can not explain

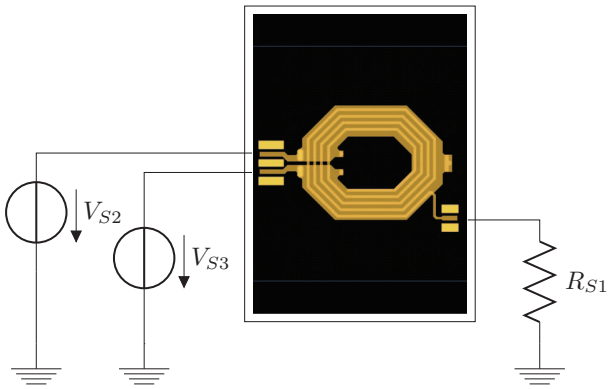

Fig. 4. Test Benchmark: Simple circuit with the balun device. The RF input signals V_{S2} and V_{S3} are are sinusoidal ones operating with 1GHz frequency. The RF output is given as current through the resistance R_{S1}.

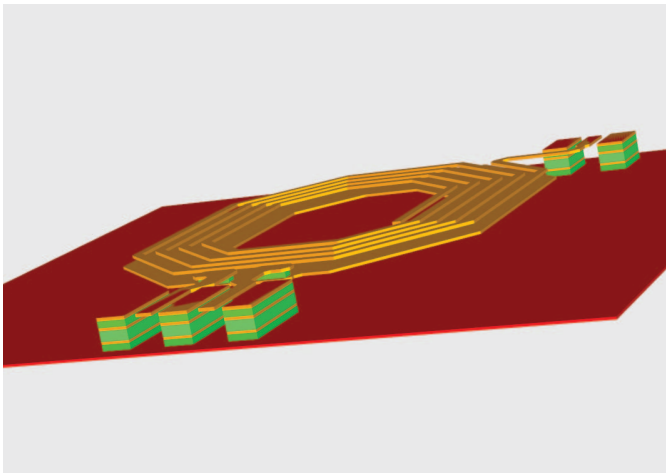

Fig. 5. Balun structure (visualization does not apply stretching in the vertical direction

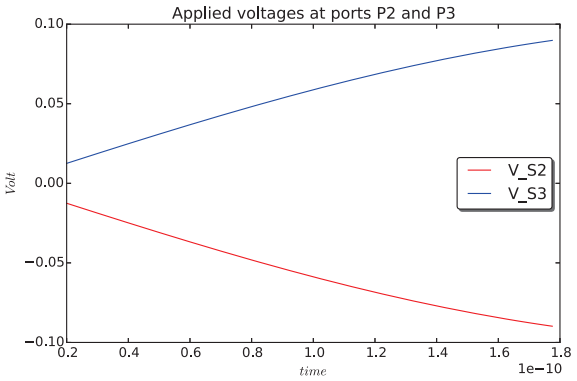

Fig. 6. Applied voltages at ports P2 and P3.

the reason for this. It could be caused by the solver or by the design of the balun.

In the transient stage we can also get a detailed view of all variables such as the current density, the electrical potential,

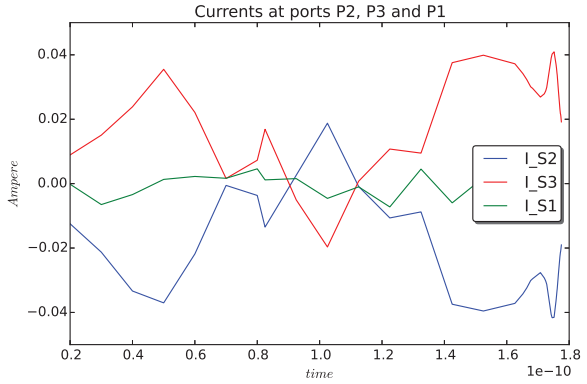

Fig. 7. Currents at ports P2 and P3 and P1.

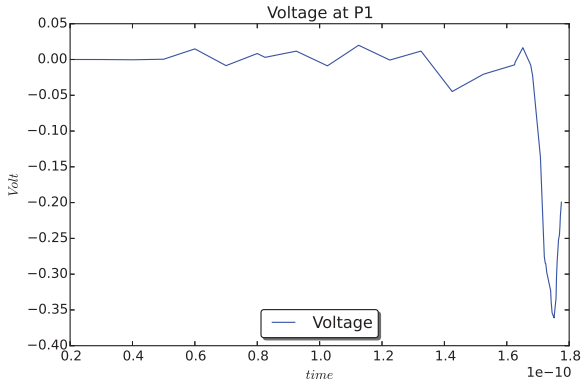

Fig. 8. Voltage at port P1.

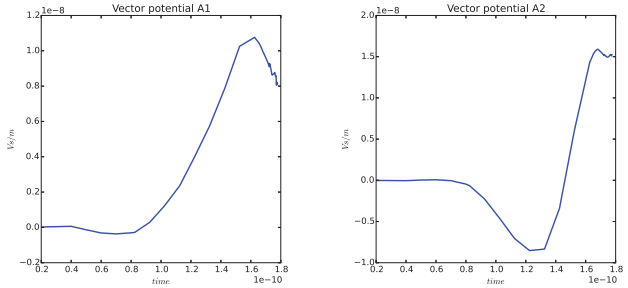

Fig. 9. Vector potentials A_1 and A_2.

the vector potential. As an example we present the magnetic inductance at $y = 2500$ micron in Figure 11 and for the open circuit coil in Figure 12.

V. Conclusion

We introduced a holistic coupled field circuit simulation and tested it with a non-trivial balun device in a simple circuit structure. We have shown that the coupled solver is based on a usual circuit netlist extended by extra lines for elements modeled by 3D field equations whose geometry and materials are described in xml files. The test benchmark shows some

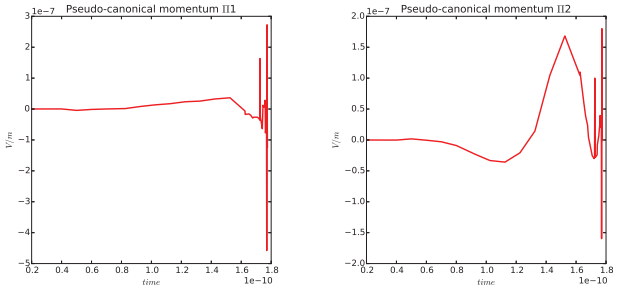

Fig. 10. Pseudo-canocnical momenta Π_1 and Π_2.

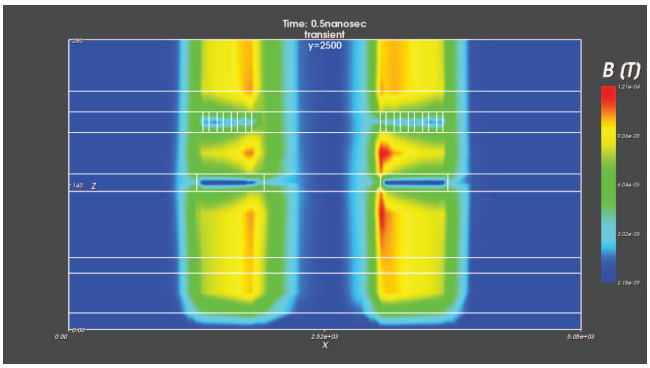

Fig. 11. Cross section of the magnetic inductance at $y = 2500$ micron.

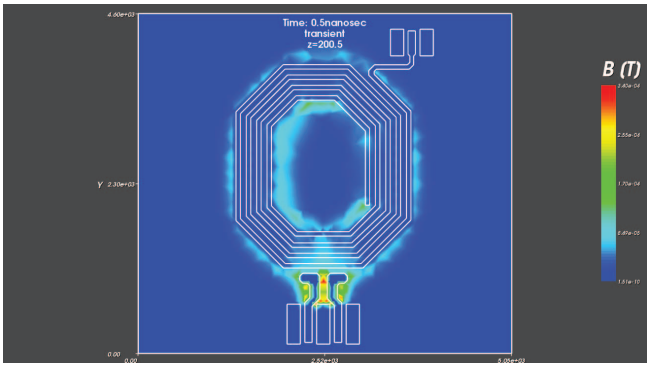

Fig. 12. Magnetic inductance in the open circuit coil.

instabilities at a certain time point. It is a task for the future to find the reasons for this instability.

Acknowledgment

This work is financially supported by the EU funded FP7 ICT project nanoCOPS GA619166. We thank Pascal Rainier from ACCO Semiconductor (France) for providing the balun structure and Kai Bittner from Fachhochschule Oberösterreich (Austria) for his valuable support for getting the holistic approach operational.

References

[1] P. Meuris, W. Schoenmaker, and W. Magnus, "Strategy for electromagnetic interconnect modeling," *Computer-Aided Design of Integrated*

Circuits and Systems, IEEE Transactions on, vol. 20, no. 6, pp. 753–762, Jun 2001.

[2] P. Markowich, *The Stationary Semiconductor Device Equations*. Springer, Wien, 1986.

[3] W. Schoenmaker, Q. Chen, and P. Galy, "Computation of self-induced magnetic field effects including the lorentz force for fast-transient phenomena in integrated-circuit devices," *Computer-Aided Design of Integrated Circuits and Systems, IEEE Transactions on*, vol. 33, no. 6, pp. 893–902, June 2014.

[4] D. Estévez Schwarz and C. Tischendorf, "Structural analysis of electric circuits and consequences for mna," *Internat. J. Circ. Theor. Appl.*, vol. 28, no. 2, pp. 131–162, 2000.

[5] S. Baumanns, *Coupled Electromagnetic Field/Circuit Simulation. Modeling and Numerical Analysis.* Logos Verlag, Berlin, 2012, Dissertation, Universität zu Köln.

[6] S. Schöps, H. De Gersem, and A. Bartel, "A cosimulation framework for multirate time integration of field/circuit coupled problems," *Magnetics, IEEE Transactions on*, vol. 46, no. 8, pp. 3233–3236, 2010.

[7] ——, "Higher-order cosimulation of field/circuit coupled problems," *Magnetics, IEEE Transactions on*, vol. 48, no. 2, pp. 535–538, 2012.

[8] C. W. Gear, "Simultaneous numerical solution of differential-algebraic equations," *IEEE Trans. Circuit Theory*, vol. CT-18, no. 1, pp. 89–95, 1971.

[9] E. Hairer and G. Wanner, *Solving Ordinary Differential Equations II: Stiff and Differential–Algebraic Problems*, ser. Springer Series in Computational Mathematics 14. Springer-Verlag, Berlin, Heidelberg, 1991.

[10] L. Petzold and P. Lötstedt, "Numerical solution of nonlinear differential equations with algebraic constraints ii: Practical implications," *SIAM Journal on Scientific and Statistical Computing*, vol. 7, no. 3, pp. 720–733, 1986.

[11] C. Tischendorf, "Solution of index-2 differential algebraic equations and its application in circuit simulation," Ph.D. dissertation, Humboldt-Universitat zu Berlin, 1996.